The oxidation rate of $(U_{0.7}Pu_{0.3})O_{2-x}$ with two fcc phases

K. Suzuki [a,*], M. Kato [a], T. Tamura [b], S. Aono [a], M. Kashimura [a]

[a] *Nuclear Fuel Cycle Engineering Laboratories, Japan Atomic Energy Agency, 4-33 Muramatsu, Tokai-Mura, Ibaraki 319-1194, Japan*
[b] *Inspection Development Company, 4-33 Muramatsu, Tokai-Mura, Ibaraki 319-1194, Japan*

Abstract

The kinetics of the oxidation in hypo-stoichiometric MOX with 30%Pu content was investigated using thermal gravity and differential thermal analysis to evaluate the variation of oxygen-to-metal ratio (O/M) in the fuel fabrication process. In the isothermal oxidation examination, the O/M ratio of the MOX gradually approached 2.00 at temperatures below 200 °C. Therefore it was considered that the oxidation reaction below 200 °C proceeded by increasing the amount of fcc phase with O/M = 2.00. Finally, the oxidation rate of hypo-stoichiometric MOX was evaluated, and the effective oxygen chemical diffusion coefficient was estimated.
© 2007 Elsevier B.V. All rights reserved.

Keywords: Diffusion; Kinetics; Nuclear materials; Oxide materials

1. Introduction

It is well known that plutonium and uranium mixed oxide (MOX) fuels having the fluorite structure are stable in the range of hyper- and hypo-stoichiometric compositions. MOX fuels have been prepared and used with hypo-stoichiometric composition for controlling the fuel and cladding chemical interaction (FCCI). Therefore the oxygen-to-metal ratio (O/M) must be strictly controlled in the fuel fabrication process as one important fuel specification.

It was reported that MOX pellets of hypo-stoichiometric composition were oxidized at room temperature in an atmosphere of inert gas and air [1,2]. It is important for the fuel fabrication process to evaluate the kinetics of the oxidation around room temperature. However, there are few data for the oxygen chemical diffusion coefficient in the hypo-stoichiometric composition region for temperatures lower than 200 °C. In this work, the oxidation rate of $(U_{0.7}Pu_{0.3})O_{2-x}$ with two fcc phases was investigated using a thermogravimetric technique at temperatures lower than 150 °C to advance understanding of the oxidation behavior.

2. Experimental

2.1. Sample preparation

The samples were prepared by a mechanical blending method [3]. The MOX powder was pressed, de-waxed (800 °C for 2 h in Ar/5%H₂) and sintered (1700 °C for 2 h in Ar/5%H₂) into pellets. The sintered pellets (85–90% theoretical density) had a number of stable pores, which were formed by crystallo-cellulose (a pore-former additive). The pellets were sliced into disc-like samples with about 1 mm thickness and then annealed under appropriate conditions to adjust the O/M ratio to 1.95–1.97 [4]. Initial characterization and impurity of the samples are shown in Tables 1 and 2, respectively.

2.2. Experimental procedure

The non-isothermal and isothermal oxidation examinations were carried out by thermal gravity and differential thermal analysis (TG–DTA). The details of the system used were described previously [4]. The isothermal oxidation was measured at 60, 125 and 150 °C in an atmosphere of air with added moisture of 1–700 ppm. The air with moisture of 700 ppm would be similar to the atmosphere found in the glove box used in the fabrication process. The sample weight change of ±1 μg which corresponds to the O/M ratio change of ±0.0002, could be measured by TG analysis with a horizontal differential type balance. The O/M ratio was calculated from the weight change of the sample using eq. (1) [4]:

$$\frac{O}{M} = 2.0000 - 16.894 \frac{\Delta W}{W} \tag{1}$$

where ΔW is the change of weight and W is the sample weight at O/M ratio of 2.0000.

The X-ray diffraction (XRD) patterns of a sample with initial O/M ratio of 1.96 were measured with time during keeping it in air at room temperature.

* Corresponding author. Tel.: +81 29 282 1111; fax: +81 29 282 3242.
E-mail address: Suzuki.kiichi@jaea.go.jp (K. Suzuki).

Table 1
Initial characterization of the samples

Item	Range
Total porosity (%)	10–15
Open porosity (%)	8–12
Closed porosity (%)	3–6
Grain size (μm)	5–7

Table 2
Impurity in the samples

Element	Content (ppm)
C	<30
N	<50
F	<10
Cl	<10
Al	<100
B	<5
Ca	<30
Cd	<5
Cr	<50
Fe	160
Mg	<15
Ni	<50
V	<50
Cu	<10
Si	<100
Zn	<100
Ag	<5
Mn	<20
Mo	<50
Pb	<30
Sn	<30

The sample surface was observed with a secondary electron microscope (SEM) before and after oxidation at 150 °C for 60 min.

3. Results

Fig. 1 shows the results of non-isothermal oxidation examination of a sample heated from room temperature to 600 °C at a constant rate of 5 °C/min. The oxidation of the sample with hypo-stoichiometric composition proceeded in two stages.
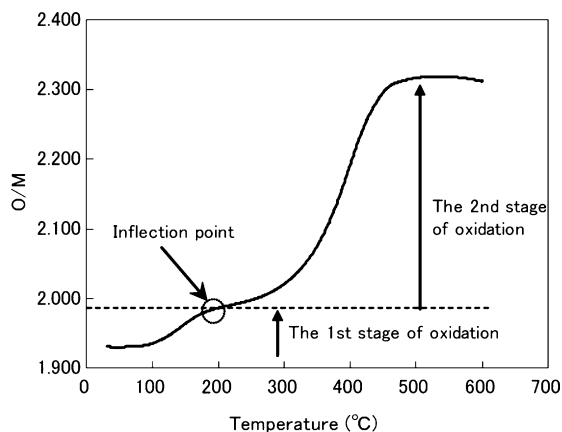
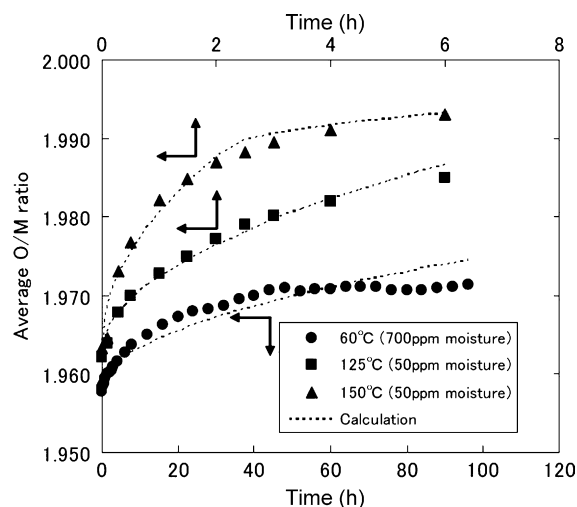Fig. 1. Results of non-isothermal oxidation examination of a sample at heating rate of 5 °C/min.

Fig. 2. Kinetics of the oxidation reaction in air plotted as a function of time and temperature.

The first stage of oxidation was dominant at temperatures below 200 °C and the O/M ratio of the sample rose to about 2.0. In the second stage of oxidation which was dominant above 200 °C, the O/M ratio of the sample increased to about 2.3.

Fig. 2 shows the kinetics of the isothermal oxidation reaction in air as a function of time and temperature. In the isothermal oxidation examination below 150 °C, the oxidation rate increased with temperature. Also, it was observed that the O/M ratio increased, approaching about 2.0.

Fig. 3 shows the diffraction patterns with time of a sample with initial O/M ratio of 1.96 which was stored at room temperature. The diffraction peak intensity of the phase with O/M = 2.00 was observed to increase with time. Other diffraction peaks such as M_4O_9 and M_3O_8 phase, which indicate an O/M ratio value greater than 2.0, were not observed.

Fig. 4 shows the SEM image of the sample surface which was oxidized at 150 °C for 60 min. Microcracks were observed on the surface of the oxidized sample, although these were not observed on the surface of the sample before the oxidation step.

4. Discussion

The isothermal oxidation in this work was mainly dominated by the first stage of oxidation as shown in Fig. 1, because the isothermal examination temperatures were less than 200 °C. The results of isothermal oxidation examination showed that the O/M ratio of sample increased, approaching 2.0 as shown in Fig. 2. In the results of XRD measurements, fcc phase with the O/M ratio of about 2.0 increased when the sample was kept in air, and other peaks were not observed. These results suggested that the oxidation in the temperature below 200 °C was dominated by the first stage of oxidation and the O/M ratio gradually approached about 2.0.

It was reported that $(U_{0.7}Pu_{0.3})O_{2-x}$ consisted of two fcc phases with different O/M ratios at room temperature, and their O/M ratios were estimated to be 1.85 and 1.985 [5,6]. The Pu–U–O ternary phase diagram in these report indicated that the increase of O/M ratio toward 2.0 for $(U_{0.7}Pu_{0.3})O_{2-x}$ with
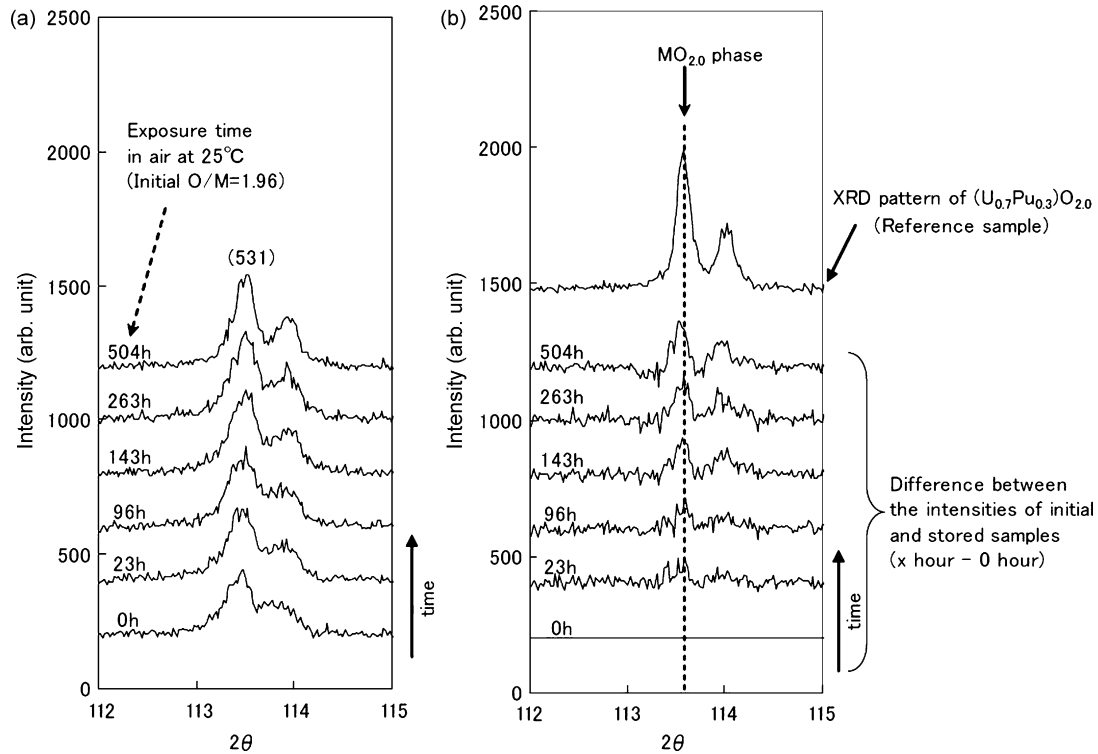
Fig. 3. X-ray diffraction patterns for sintered MOX sample. (a) Change of diffraction peaks for (531). (b) Change of differences between the intensities of initial and stored samples.

two fcc phases was caused by increasing the amount of single fcc phase with O/M ratio of 1.985–2.00. The O/M ratios of the samples used in the present work were from 1.95 to 1.97, so samples consisted of two fcc phases. It seemed that the fcc phase which appeared with time (shown in Fig. 3) corresponded to the phase with the higher O/M ratio in the two fcc phase region. Therefore, the oxidation of $(U_{0.7}Pu_{0.3})O_{2-x}$ with two fcc phases could be understood by diffusion of the higher O/M ratio phase formed on the sample surface.

Jost [7] treated diffusion in a system consisting of two phases as shown in Fig. 5. The distribution of O/M ratios was expressed

by the following equation as a function of x:

$$\frac{O}{M_x} = \frac{O}{M_s} - B \, erf \left(\frac{x}{2\sqrt{\tilde{D}t}} \right) \quad \text{for } 0 < x < \xi \tag{1}$$

$$\frac{O}{M_x} = \frac{O}{M_i} \quad \text{for } x \geq \xi \tag{2}$$

Here O/M_x is the O/M ratio at x, O/M_s the O/M ratio on the sample surface, O/M_i the initial O/M ratio, B the arbitrary constant, t the time, $\tilde{D}$ the oxygen chemical diffusion coefficient and ξ is the discontinuous point of O/M ratio distribution. The kinetics of the oxidation was evaluated to estimate the oxygen chemical diffusion coefficient by using Eq. (1) as shown in Fig. 2. In the calculation, O/M_s was assumed to be 2.0 and the calculation
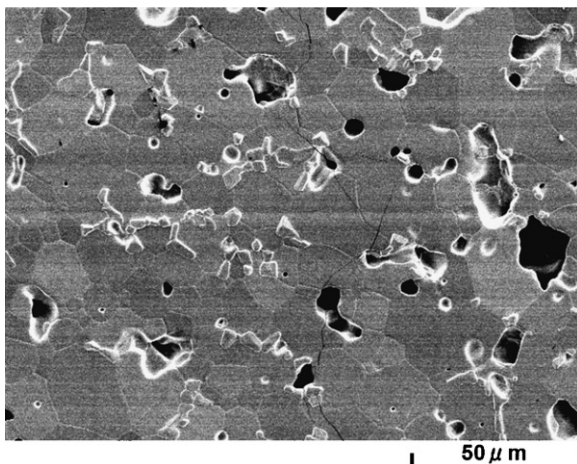

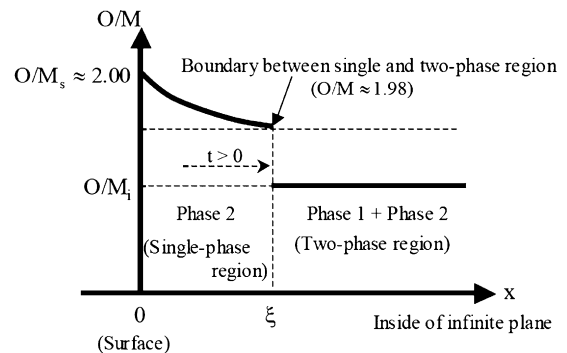Fig. 4. SEM image of sample surface which was oxidized at 150 °C for 60 min.

Fig. 5. Diffusion into the two-phase system. Discontinuous point of O/M distribution ξ is located on the surface for $t = 0$, where Phase 1 = the lower O/M phase and Phase 2 = the higher O/M phase.
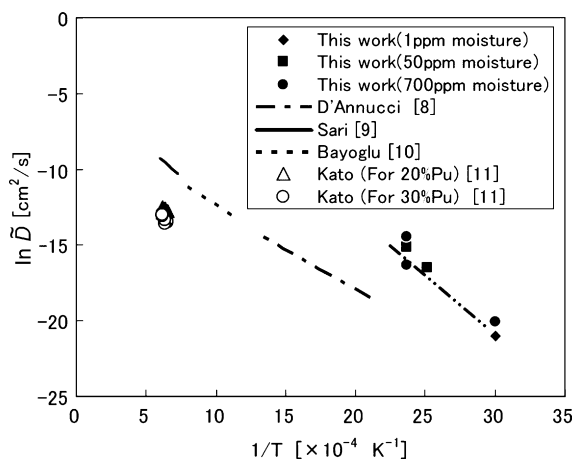
Fig. 6. ln $\tilde{D}$ plotted against reciprocal temperature.

results were in good agreement with experimental values when the higher O/M ratio was assigned as 1.98 (Fig. 5).

The obtained diffusion coefficients are plotted in Fig. 6. The oxygen chemical diffusion coefficient in air was expressed by the following equation as a function of inverse temperature:

$$\tilde{D} = 3.92 \times 10^2 \exp\left(-\frac{73.4 \times 10^3}{RT}\right) \text{ cm}^2\,\text{s}^{-1} \qquad (3)$$

Here R is the gas constant and T is the temperature. The activation energy of the diffusion, ΔH, of $(U_{0.7}Pu_{0.3})O_{2-x}$ was obtained as 73.4 kJ/mol. The activation energies of oxygen diffusion in MOX have been reported to be 43.5–88.9 kJ/mol [8–11], which were approximately the same as the value obtained in this work.

Oxygen chemical diffusion coefficients measured by other works are also plotted in Fig. 6 [8–11]. The results of this work were much larger than the literature data. To explain this result, it would be necessary to assume a fast diffusion mechanism. Microcracks were observed in the oxidized sample as shown in Fig. 4. It was reported that the lattice parameter of MOX decreased with an increase of O/M ratio [12]. It seemed in this work that the oxidation of MOX decreased the lattice parameter and caused stress which led to microcracks on the surface. The existence of the microcracks would accelerate oxidation of sintered MOX. However, it was not possible to explain a very large oxygen chemical diffusion coefficient only by existence of microcracks. It was reported that grain boundary diffusion affected migration rate at comparatively low temperature in various materials on behalf of volume diffusion [13–15]. It seemed that grain boundary diffusion was also important in the oxidation of MOX at comparatively low temperature. Moreover, the initial open porosity of the samples was about 8–12%, and this would have an impact on the oxidation rate. The oxygen chemical diffusion coefficient obtained in this work might be the effective chemical diffusion coefficient which was accelerated by microcracks, grain boundary diffusion and open porosity.

Woodley and Gibby [1] reported that oxidation rate increased with an increase of the moisture concentration at the very low moisture concentrations (1–2 ppm) and saturated at moisture concentrations higher than about 10 ppm. However, the present work could not confirm the effect of moisture concentration in the atmosphere on the diffusion coefficient due to a lack of experimental data.

5. Conclusion

The oxidation behavior of $(U_{0.7}Pu_{0.3})O_{2-x}$ with two fcc phases was investigated. The oxidation of hypo-stoichiometric MOX proceeded in two stages with an inflection point at 200 °C. It was observed that the oxidation proceeded by increasing the amount of fcc phase with O/M ratio of about 2.00, and the O/M ratio of MOX pellets was not expected to exceed O/M = 2.00. The kinetics of the oxidation was evaluated to estimate the diffusion coefficient using the model of diffusion in a system consisting of two phases. A very large coefficient of oxygen chemical diffusion was estimated in $(U_{0.7}Pu_{0.3})O_{2-x}$, which was expected to be the effective chemical diffusion coefficient accelerated by microcracks, grain boundary diffusion and open porosity.

Acknowledgements

References

[1] R.E. Woodley, R.L. Gibby, HEDL-SA-592, 1973.
[2] R. Eichler, D. Hanus, J. Krellmann, R. Löb, H. Roepenack, J. Nucl. Mater. 124 (1984) 9.
[3] K. Asakura, K. Takeuchi, J. Nucl. Mater. 348 (2006) 165.
[4] M. Kato, T. Tamura, K. Konashi, S. Aono, J. Nucl. Mater. 344 (2005) 235.
[5] C. Sari, U. Benedict, H. Blank, J. Nucl. Mater. 35 (1970) 267.
[6] M. Kato, H. Uno, T. Tamura, K. Morimoto, K. Konashi, Y. Kihara, Proceedings of Actinides 2005, vol. 108, Manchester, 4P04, 2004.
[7] W. Jost, Diffusion in Solids, Liquids and Gases, Academic Press, Inc., 1960, p. 69.
[8] F. D'annucci, C. Sari, J. Nucl. Mater. 68 (1977) 357.
[9] C. Sari, J. Nucl. Mater. 78 (1978) 425.
[10] A.S. Bayoglu, Solid State Ionics 12 (1984) 53.
[11] M. Kato, K. Morimoto, T. Tamura, T. Sunaoshi, K. Konashi, S. Aono, M. Kashimura, Proceedings of Plutonium Futures The Science, Asilomar, Pacific Globe, California, US, July 9–13, 2006, 2006.
[12] T.L. Markin, R.S. Street, J. Inorg. Nucl. Chem. 29 (1967) 2265.
[13] D. Turnbull, Atom Movement, ASM, Cleveland, 1951.
[14] N.N. Khoi, W.W. Smeltzer, J.D. Embury, J. Electrochem. Soc. 122 (1975) 1495.
[15] A. Atkinson, R.I. Taylor, Philos. Mag. A43 (1981) 979.